Volume-4, Issue-9, Sept-2015 • ISSN No 2277 - 8160

Research Paper | Medical Science

Development of a Pattern Recognition System For Discriminating Osteoarthritic Bone Marrow Edema Like Lesions on MRI

Georgios Katsiberis	Radiologist, Department of Radiology, School of Medicine, University of Patras, Rio, GR-26503 Greece
Pantelis Georgiadis	Radiologist, Department of Radiology, School of Medicine, University of Patras, Rio, GR-26503 Greece
Aspasia Rigopoulou	Radiologist, Department of Radiology University Hospital of Patras, School of Medicine, University of Patras, Rio, GR-26503 Greece
Dimitrios Siamplis	Professor, Department of Radiology, School of Medicine University of Patras, School of Medicine, University of Patras, Rio, GR-26503 Greece
Elias Panagiotopoulos	Professor, Orthopaedic School of Medicine University of Patras, School of Medicine, University of Patras, Rio, GR-26503 Greece
*** Ekaterini Solomou**	Associate professor Department of Radiology, School of Medicine University of Patras, MRI Department of University Hospital of Patras, Rio, GR-26503 Greece. * Corresponding author

ABSTRACT

A non-invasive method developed to investigate the capacity of digital image texture analysis for the detection and differentiation of hip ostaoarthritic lesions.

Thirty one femoral heads, after hip arthroplasty, were examined on a 1.5T MRI system. Bone marrow lesions (edema and cysts) were graded on MRI. Utilizing these MRI series, volumes of interest were extracted and classified for every ostaoarthritic lesion.

According to the developed pattern recognition system, the highest classification accuracy in discriminating bone marrow edema from bone cysts was 98,92%, employing five textural features (mean value, correlation, sum of squares, sum average and sum variance). Individual accuracies in classifying correctly bone marrow edema lesions were 98, 73% and bone cysts 99, 07%.

Using the developed pattern recognition system, accurately grading the severity of hip osteoarthritis can be performed, discriminating reversible and irreversible lesions in order to monitor the progression of the disease and the therapy effectiveness.

KEYWORDS : bone cysts- oedema; MRI; osteoarthritis; pattern classification; textural features

INTRODUCTION

Osteoarthritis (OA) is one of the most common musculoskeletal diseases associated mainly with aging.

The clinical symptoms include pain, joint stiffness and rigidity, motion dysfunction and in chronic stages it causes joint deformity [1,2].

In the development process of OA, articular cartilage changes play a key role, such as the loss of hyaline articular cartilage and the degradation of proteoglycans (PGs) [1,3].

Articular cartilage damage causes changes in the underlying bone and the joint margins[1].

It is suggested that early diagnosis of OA is important for clinical treatment and therefore the quantitative evaluation of the biochemical compositional changes of cartilage which occur before morphologic degradation is valuable for the early diagnosis of OA.

Osteoarthritis of the hip is a multifactorial process and hip pain associated with OA is the most common cause of pain in older adults. Prevalence studies have shown the rates for adult hip OA range from 0.4% to 27%. The major predisposing factors are age, developmental disorders, race, gender, genetics, occupation, sports exposure and previous injury [2].

HIP OA alterations: bone marrow oedema-like signal lesions

Osteoarthritis associated with bone marrow oedema-like signal lesions is an expression of a number of non-characteristic histologic abnormalities that include bone marrow necrosis, bone marrow fibrosis, and trabeculae abnormalities. Subchondral bone marrow signal alterations may be observed in conjunction with trauma, chronic cartilage damage and osteoarthritis, as an idiopathic entity or as a feature of other diseases, such as osteonecrosis, inflammation or tumor. In OA, the importance of subchondral bone marrow signal alterations for structural progression, as well as a cause of pain, has been discussed in the literature. Most of these lesions are associated with overlying cartilage damage.

Subchondral cystic lesions appear as well-defined areas of fluid signal on Magnetic Resonance Imaging (MRI), which can be associated with osteoarthritis.

In OA research, bone marrow lesion (BML) size is regularly assessed with quantitative and qualitative methods.

Modality

Magnetic resonance imaging (MRI) is a noninvasive multiplanar sensitive and useful method that can detect the changes of cartilage degeneration and other osteoarthritic changes. With its ability to visualize cartilage, soft tissues and bone, MRI is the method of choice for

the assessment of acute and chronic joint disorders [3].

Several MRI techniques are available including T1, T2 and Fat saturated weighted images and also delayed gadolinium-enhanced MRI for the cartilage abnormalities.

T2 and fat sat images are widely used and have been proven to be more sensitive to collagen changes in the cartilage.

The use of a panel of biomarkers for quantification is certainly the next step in quantitative MRI.

Aim

In the literature there are many radiological grading systems for OA lesions. Traditional scoring systems developed for X-ray are not applicable to the new data of MRI studies. Accepted scoring methods designed for MRI are predominantly qualitative and are based on visual assessment of the data without further grading according to objective grading system. The qualitative analysis can provide useful information of the OA lesion and inflammation, but there is lack of objectivity.

Emerging quantitative computer-aided methods present a new approach to monitoring disease activity and evaluating the effect of treatment.

Until now, in the literature, there are a few imaging analysis systems grading the severity of OA using X-rays. Boniatis et al. created a computer-aided classification system, based on X-Rays, for the assessment of the severity of hip osteoarthritis [4], whereas Gregory et. al. developed an active shape model of the proximal femur to determine whether morphological changes of the bone could be quantified by using as a marker of hip OA [5].

Although it is very important to detect early OA lesions, especially reversible bone marrow lesions in order to prevent progression of the disease, according to our knowledge, there is no previous work for the evaluation and the differentiation of OA lesions with a pattern recognition system based on MRI.

The purpose of the present study was to detect lesions of the bone marrow with MRI and to develop a pattern recognition system to identify and differentiate BMLs lesions in order to provide the appropriate therapy.

MATERIALS AND METHODS

Thirty one patients were submitted in total hip arthroplasty due to severe osteoarthritis. All femoral heads were examined on a 1.5T MRI system (GE HDX Signa) using a commercially available polarized knee coil after obtaining informed consent, according to the Helsinki Declaration and after our institutional review board approved this study. MR images were acquired using the T1 water excitation three dimensional (T1 3D FSPGR SPECIAL) sequence with repetition time: 20.6ms, echo time: 10ms, flip angle: 12, field of view: 160mm, slice thickness/interslice gap: 1.6mm/0.7mm, matrix: 512x512, phase encoding: right to left.

T1 Spin Echo weighted images (wi) were also obtained using repetition time: 860ms, echo time: 13ms, field of view: 100mm, slice thickness/interslice gap: 2.0mm/0.2mm, matrix: 256x192, phase encoding: anterior to posterior.

Additionally, T2 Fast Recover Spin Echo sequences were acquired using repetition time: 6440ms, echo time: 42ms, field of view: 100mm, slice thickness/interslice gap: 2.0mm/0.2mm, matrix: 384x256, phase encoding: anterior to posterior.

Subchondral bone marrow oedema-like signal alterations exhibit typical signal characteristics on MRI and are common but non-specific findings of OA. MRI is the gold standard method to assess bone marrow, as early bone marrow damage cannot be visualized with any other techniques such as X-ray or ultrasound. On MRI, subchondral bone marrow signal alterations are visualized as ill-defined low signal intensity lesions on T1 weighted images compared to the unaffected bone marrow (Figure 1).

On T2, proton density (PD) and fat suppressed (FS) weighted images these lesions are characterized as ill-defined areas of high signal intensity in the subchondral cancellous bone, extending from the articular surface to a variable distance (Figure 2).

In order to classify oedema, we used the grading system of Kornaat et al. [3] and the lesions were graded as following: grade 0, absent; grade 1, minimal (diameter <5 mm); grade 2, moderate (diameter 5 mm to 2 cm); grade 3, severe (diameter >2 cm) (Figure 2).

Subchondral cysts were defined as clearly delimited areas of high signal intensity on T2 wi with sclerotic margins, in the cancellous bone. According to their greatest dimension they were graded as: grade 0, normal; grade 1, minimal (<3 mm); grade 2, moderate (3–5 mm); grade 3, severe (>5 mm) (Figure 3), according to the Kornaat et al. score [3].

Volume of Interest Extraction and Textural Features Calculation

Utilizing these MRI series, an expert radiologist specified cubic Volumes of Interest (VOIs) within each OA lesion using a software program, developed for the purposes of the present study. The program was designed using the C++ programming language and the Visualization Tool Kit (VTK) [6]. By utilizing the marching cubes algorithm [7], 3-dimensional models were built from DICOM MRI-series, providing the radiologist with a visual aid in order to segment the VOIs with lesions. From each segmented MRI-VOI, a set of parameters (features) that quantified the properties of volume-texture within the lesion was calculated.

Haralick et al. [8] and Galloway [9] described a set of textural features, based on the gray-level co-occurrence and run-length matrices that quantified textural properties of 2D images. Their 3D (volumetric) equivalents [10, 11] were employed in the present study for the purpose of quantifying textural volume properties of OA lesions. Additionally, this set was enriched with features derived from the VOI's histogram (mean value, standard deviation, skewness and kurtosis). Thus, a set of 36 volumetric textural features was extracted for each lesion; 4 from the VOI's histogram, 22 from the co-occurrence and 10 from the run-length matrices (Table 1).

All features were normalized to zero mean and unit standard deviation [12], according to Equation 1

$$x_i' = \frac{x_i - m}{std} \qquad (1)$$

where x_i and x_i' are the *i*-th feature values before and after the normalization respectively, and *m* and *std* are the mean value and standard deviation, respectively, of feature x_i over all patterns and all classes.

Least squares feature transformation - Probabilistic neural network classifier (LSFT-PNN)

Due to the small size of the dataset utilized in the present study, the probabilistic neural network (PNN) classifier was chosen. The PNN is a non-parametric feed-forward neural network classifier that encompasses both the Bayes' classification approach and the Parzen's estimators of probability density functions [13]. The decision function of the PNN classifier is described by:

$$d_k(x) = \frac{1}{(2\pi)^{\frac{n}{2}}\sigma^n N_k} \sum_{i=1}^{N_k} e^{-\frac{\|x-x_i\|^2}{2\sigma^2}} \qquad (2)$$

where x_i is the i_{th} training input pattern, x is the unknown pattern to be classified, N_k is the number of patterns forming the class x_k, n is the number of textural features forming the input pattern while sigma σ is an adjusting parameter, taking values ranging between 0 and 1.

According to Equation 2, as the distance between x and x_i ($\|x-x_i\|$) increases, the exponential term approaches 0, indicating a small similarity between the two pattern vectors. On the other hand, as the distance between x and x_i ($\|x-x_i\|$) decreases, the exponential term approaches 1, indicating a significant similarity between the two pattern vectors. As σ approaches 0, even small differences between x_i and x

will provide a zero value for the exponential term, while larger values of sigma provide more smooth results. The selection of sigma affects the estimation error of the PNN and in the present study was determined experimentally by comparing the accuracies obtained for different values of the parameter. The unknown pattern *x* is classified to the class with the highest value of decision function $d_k(x)$ [13].

As presented in Figure 4, the basic PNN architecture consists of an input layer, a pattern layer, a summation layer and an output layer. The input layer stores temporarily each pattern vector, which is fed to the network. The number of neurons (nodes) that structure the input layer is equal to the dimensionality of the input pattern. Each input pattern is mapped to each one of the neurons of the pattern layer. Each neuron in the pattern layer represents a training pattern. In the pattern layer, the Euclidean distance between the input and each training pattern is computed. The decision function (Equation 2) is then applied to provide the output of the pattern neuron. The summation layer has one neuron for each class, and implements the summation term of Equation 2 for the outputs of the patterns corresponding to the class. As it can be observed, each summation neuron is connected to the neurons of the corresponding pattern layer. The output layer contains one neuron and assigns the input vector to a class by implementing a classification rule. In particular, the unknown pattern is classified to the class with the highest value of decision function $d_k(x)$ [13].

Training patterns x_i, prior to entering the PNN classifier, were transformed by means of a non-lineal least squares feature transformation (LSFT) technique, to render classes more separable by clustering the patterns of each class around arbitrary pre-selected points. The utilized LSFT method is an extension of the linear least squares mapping technique, introduced by Ahmed and Rao [14].

Classification Scheme Design

An LSFT-PNN based classification scheme was designed to discriminate between bone marrow oedema and bone cysts (Figure 5).

The External-Cross-Validation (ECV) technique was used to avoid bias conditions [15], which may occur by using the same dataset in the feature selection and evaluation stages. Therefore, the dataset was randomly split in two subsets; one was used for optimal classifier design (2/3 of the dataset) and the other for evaluation (1/3 of the dataset). The optimum feature combination in the design stage was determined by employing the exhaustive search method [12]. Accordingly, the LSFT-PNN classifier was designed by all possible feature combinations (up to 5 features), and at each combination the classifier's performance was evaluated by means of the leave-one-out (LOO) method [12], i.e. the LSFT-PNN classifier was designed by all but one pattern-vector, which was considered unknown and it was classified as such. The process was repeated, each time leaving-out a different pattern-vector, until all pattern-vectors were classified to one of the two lesion classes. Thus, the optimal feature vector retained was the one that gave the highest classification accuracy with the least number of features (Figure 6).

RESULTS

All femoral heads exhibited extensive OA lesions on MRI. 30 cases were classified as grade 3 according to Kornaat classification and only 1 was classified as grade 2.

According to the subchondral cysts MRI revealed 5 femoral heads classified as grade 1, 6 cases classified as grade 2 and 20 cases graded 3.

In accordance to the designed and implemented pattern recognition system, the highest classification accuracy in discriminating bone marrow oedema from bone cysts was 98.92%, employing five textural features (mean value, correlation, sum of squares, sum average and sum variance). Individual accuracies in classifying correctly bone marrow oedema lesions were 98.73% and bone cysts 99.07%. Comparative classification results for various numbers of features are presented in Table 2.

Figure 6 depicts the boxplot of the best textural features for both bone marrow oedema (Figure 7a) and bone cysts (Figure 7b), normalized according to Equation 1. The distribution of the normalized feature values was overlaid on the boxplots, employing a gradient bar where darker parts indicate higher value occurrences. Values marked with the plus sign are outliers and the horizontal lines within the boxes indicate median values.

DISCUSSION

MRI is the gold standard method to recognize OA alterations in order to prevent the extension of the disease.

Bone marrow oedema is a reversible lesion and can be treated in early stages, thus it is extremely important to visualize and diagnose it. On the contrary, subchondral cystic lesions are signs of disease progression and cannot be reversed.

MRI, with high sensitivity to visualize bone marrow, cartilage and soft tissues, is the method of choice for the detection of OA lesions and for the assessment of acute and chronic joint disorders, as the subchondral bone marrow cannot be visualized by X-ray or ultrasound. Thus, it is very important to choose the most sensitive sequences for the detection even of the smallest bone marrow alterations. T1 3D FSPGR, T2 wi, Proton Density (PDwi), fat suppressed (FS) images are the sequences used in our study.

Bone marrow oedema was assessed as an ill-defined area of increased signal intensity in the subchondral cancellous bone, extending from the articular surface to a variable distance. On the other hand, subchondral cysts were determined as well-defined areas of high signal intensity on T2-weighted images, in the cancellous bone underlying the joint cartilage [3].

There have been several reports relating subchondral marrow edema patterns to osteoarthritis but few have correlated the association between marrow edema and subchondral cyst development. Previous studies in the literature have showed that subchondral cysts arise within regions of subchondral marrow edema-like signal and typically also subjacent to cartilage abnormalities in patients with imaging evidence of osteoarthritis or progression of osteoarthritis [1].

Bony microcontusions leading to necrosis, increased intra-articular pressure leading to extension of synovial fluid into the subchondral bone through tiny gaps in the articular surface (Bone Contusion Theory), or the proliferation of myxomatous tissue within the bone marrow (Synovial Breach Theory), are the main proposed theories in the literature for the pathogenic mechanism of subchondral cyst formation in osteoarthritis[1].

Carrino et al. supported that bone marrow edema-like signal can be an early "pre-cyst" lesion, while not every area of bone marrow edema-like signal will give rise to a cyst [1]. In our study, we used the Kornaat et al. grading system, in order to quantify bone marrow edema and subchondral lesions [3].

All femoral heads studied on MRI showed severe OA changes. Furthermore the developed pattern recognition system, gave us the opportunity to determine and characterize precisely even the smallest lesions in the bone marrow which were not obvious by other radiological methods. As mentioned above, bone marrow oedema is a reversible condition, while subchondral cysts are not. Therefore, using the pattern recognition system in combination with MRI, early detection and characterization of subchondral lesions can be achieved for grading and monitoring the stage of OA in order to choose the right therapeutic management to avoid the progression of OA.

The ECV method enabled the assessment of the system's generalization to new 'unseen' data. Under the ECV, the LSFT-PNN classification scheme achieved overall accuracy of 98.92% in discriminating bone marrow oedema from bone cysts. The textural features that optimized classification results described the signal intensity (mean value), the gray-tone linear dependencies (correlation), the dispersion of the gray-tone intensity values (sum average), and the variance of the normalized grey-tones in the spatial domain (sum variance, sum of squares).

Limitations of the study are the small number of femoral heads that were examined and the severe degree of osteoarthritic alterations.

We conclude that bone marrow edema like lesions detected on MRI can be differentiated and classified with great accuracy and specificity using the developed pattern recognition system.

Table 1. Textural features extracted.

Methods	Features
Histogram (1st order statistics)	Mean Value, Standard Deviation, Skewness, Kurtosis
Mean and range of 0°, 45°, 90° and 135° co-occurrence matrices (2nd order statistics)	Angular Second Moment, Contrast, Correlation, Sum Of Squares, Inverse Difference Moment, Sum Average, Sum Variance, Sum Entropy, Entropy, Difference Variance, Difference Entropy
Mean and range of 0°, 45°, 90° and 135° run-length matrices (2nd order statistics)	Short Run Emphasis, Long Run Emphasis, Gray Level Non Uniformity, Run Length Non Uniformity, Run Percentage

Table 2: Classification results utilizing the ECV method and the LSFT-PNN classifier.

Number of Features	Bone Marrow Edema vs Bone Cysts Overall Accuracy (%)
1	73,12
2	77,96
3	88,71
4	98,39
5	98,92

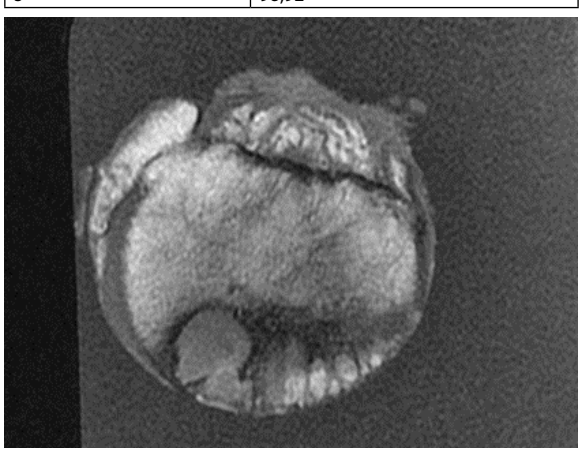

Figure 1: coronal T1 SE wi exhibits subchondral cystic lesions with intermediate signal intensity surrounded by low signal bone marrow oedema.

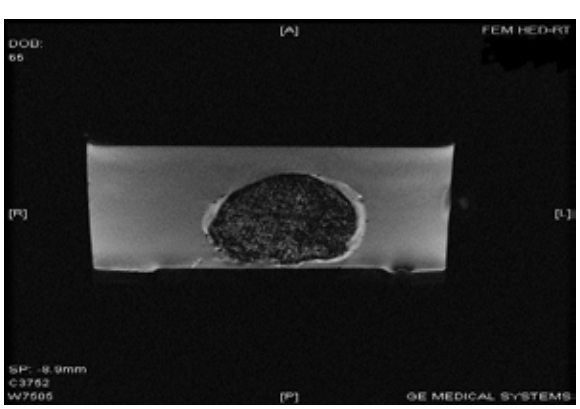

Figure 2: T1 3D FSPGR SPECIAL (water excitation), shows ill-defined areas of increased signal, suggesting bone marrow oedema, grade III according to Kornaat system.

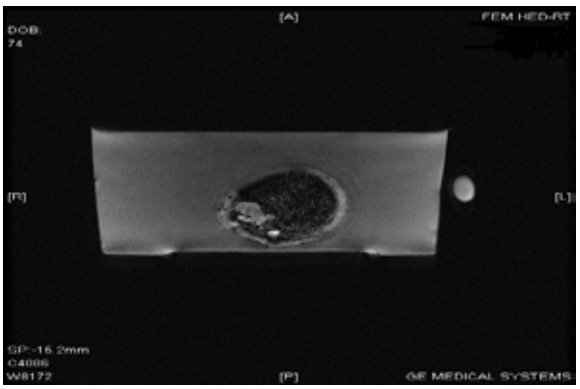

Figure 3: T1 3D FSPGR SPECIAL (water excitation) depicts well-defined cysts of high signal intensity (grade III)

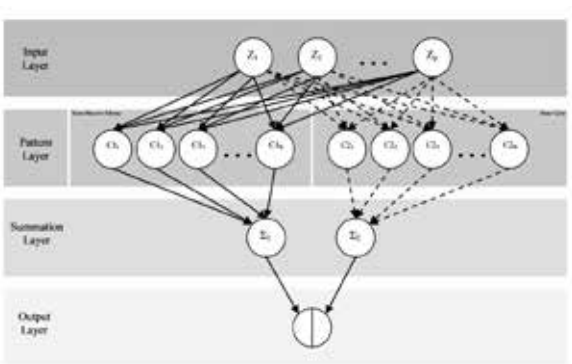

Figure 4: The basic PNN architecture.

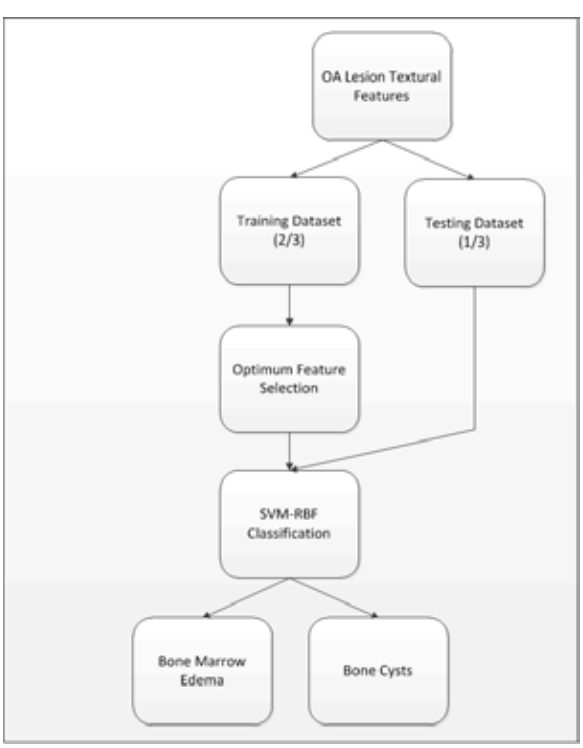

Figure 5: Classification scheme design.

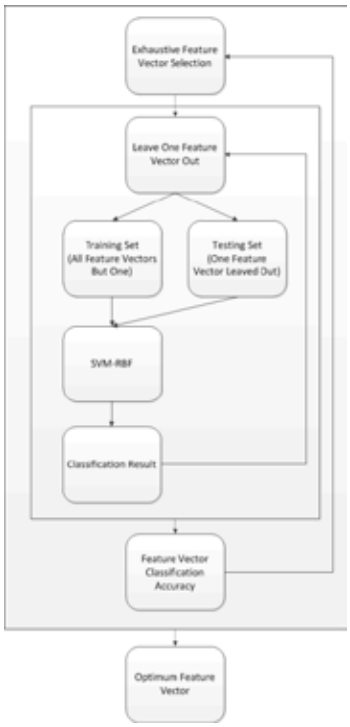

Figure 6: Optimal feature selection procedure.

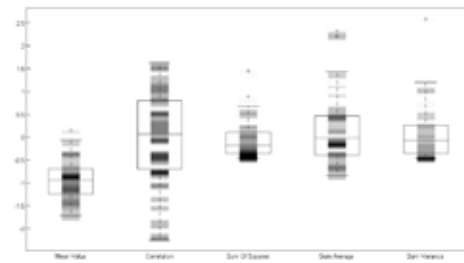

Figure 7a: Boxplot of the best textural features for bone marrow oedema.

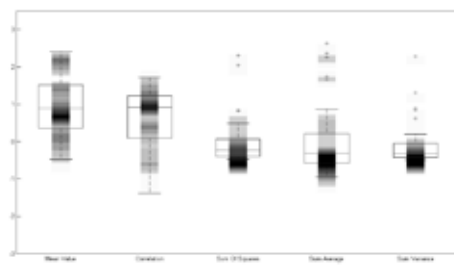

Figure 7b: Boxplot of the best textural features for bone cysts.

REFERENCES

1 Carrino JA, Blum J, Parellada JA, Schweitzer ME, Morrison WB. MRI of bone marrow edema-like signal in the pathogenesis of subchondral cysts. Osteoarthritis and cartilage / OARS, Osteoarthritis Research Society 2006;14(10):1081-5. | 2 Cibulka MT, White DM, Woehrle J, et al. Hip pain and mobility deficits--hip osteoarthritis: clinical practice guidelines linked to the international classification of functioning, disability, and health from the orthopaedic section of the American Physical Therapy Association. Journal of Orthopaedic & Sports Physical Therary 2009;39(4):A1-A25. | 3 Kornaat PR, Ceulemans RYT, Kroon HM, et al. MRI assessment of knee osteoarthritis: Knee Osteoarthritis Scoring System (KOSS)—inter-observer and intra-observer reproducibility of a compartment-based scoring system. Skeletal Radiology 2005;34(2):95-102. | 4 Boniatis IS, Costaridou LI, Cavouras DA, Panagiotopoulos EC, Panayiotakis GS. Quantitative assessment of hip osteoarthritis based on image texture analysis. Br J Radiol 2006;79(939):232-8. | 5 Gregory JS, Waarsing JH, Day J, et al. Early identification of radiographic osteoarthritis of the hip using an active shape model to quantify changes in bone morphometric features: Can hip shape tell us anything about the progression of osteoarthritis? Arthritis & Rheumatism 2007;56(11):3634-43. | 6 Schroeder WJ, Schroeder WJ, Avila LS, Hoffman W. Visualizing with VTK: a tutorial. IEEE Computer Graphics and Applications 2000;20(5):20-7. | 7 Lorensen W, Cline H. Marching cubes: A high resolution 3D surface construction algorithm. Computer Graphics 1987;21(4):163-9. | 8 Haralick RM, Shanmugam K, Dinstein I. Textural Features for Image Classification. IEEE Trans Syst Man Cybern 1973;SMC-3:610-21. | 9 Galloway MM. Texture Analysis Using Grey Level Run Lengths. Comp. Graph. and. Image Proc 1975;4:172-9. | 10 Mahmoud-Ghoneim D, Toussaint G, Constans JM, de Certaines JD. Three dimensional texture analysis in MRI: a preliminary evaluation in gliomas. Magnetic resonance imaging 2003;21(9):983-7. | 11 Xu DH, Kurani A, D. FJ, S. RD. Run-length encoding for volumetric texture. In: 4th IASTED International Conference on Visualization, Imaging, and Image Processing - VIIP 2004. Marbella, Spain. | 12 Theodoridis S, Koutroumbas K. Pattern Recognition. New York: Academic Press; 1999. | 13 Specht DF. Probabilistic Neural Networks. Neural Networks 1990;3: 109-18. | 14 Ahmed N, Rao R. Orthogonal Transforms for Digital Signal Processing. NY: Springer-Verlag; 1975. | 15 Ambroise C, McLachlan GJ. Selection bias in gene extraction on the basis of microarray gene-expression data. Proc Natl Acad Sci USA 2002;99(10):6562-6. |